Population Balances Coupled with the CFD-Code FeatFlow

Dmitri Kuzmin* Volker Mehrmann† Sonja Schlauch†
Andriy Sokolov* Stefan Turek*

June 12, 2006

Abstract

The simulation of drop size distributions in stirred liquid-liquid systems is studied. The simulation is realized via the coupling of the CFD code FeatFlow with the population balance solver Parsival. It is shown how such a coupling may be constructed and the properties of the coupled solver are critically analyzed.

1 Introduction

The control of drop size distributions in stirred liquid-liquid systems is of major interest in many fields of engineering science such as chemical, pharmaceutical, mining, petroleum, or food industries. The technical vision is to be able to achieve a desired averaged drop size and a defined drop size distribution, using control parameters such as the stirrer speed. In many technical applications, like in the production of styrofoam, for example, monodisperse systems with a certain drop size are desired. However, before being able to control the drop size distribution in a stirred tank reactor, one needs to understand, model, and simulate the processes occuring in such a system.

In this paper, we will discuss an approach for the numerical simulation of the processes in a stirred liquid-liquid system via a coupling of the CFD code FeatFlow with the population balance solver Parsival.

Since the energy dissipation rate ε is needed for the calculation of the coalescence and breakage rates in Parsival, these values have to be provided by the flow simulation. For this reason the k-ε turbulence model solver **Pp3d-Ke** is used from the list of solvers offered by FeatFlow. This method solves

*Institut für Angewandte Mathematik, Universität Dortmund, Vogelpothsweg 87, D-44227 Dortmund, Email addresses: kuzmin@math.uni-dortmund.de, asokolow@math.uni-dortmund.de, stefan.turek@math.uni-dortmund.de.

†Institut für Mathematik, Technische Universität Berlin, Straße des 17. Juni 136, D-10623 Berlin. Email addresses: mehrmann@math.tu-berlin.de, schlauch@math.tu-berlin.de.

the Reynolds-averaged Navier-Stokes equations plus two transport equations for the turbulent kinetic energy k and its dissipation rate ε. The special features of FeatFlow that are needed for the simulation of the considered application and, in particular, for the coupling approach, namely the treatment of moving boundaries as well as the integration of a k-ε turbulence model, are described in Section 2. However, the use of FeatFlow extended by the k-ε model within this coupling approach is very sophisticated, see Section 3. We will describe some of the current and future challenges in Section 4.

2 New features of FeatFlow

2.1 Moving boundaries

A 3D finite element solver for the incompressible Navier-Stokes equations with moving boundary parts is provided in the module **Pp3d_Movbc** of the open-source CFD code FeatFlow. This module is based on iterative filtering techniques in combination with fictitious boundary conditions that are used to implement the moving tread patterns. All calculations are performed on one mesh which does not change in time. From a geometrical point of view, this approach is successful even together with the prescribed complex tread patterns such that MPEG movies can demonstrate the realistic movement of these patterns. More detailed analysis and a way of realization can be found in [TDR02]. However, the moving boundary method for the k-ε turbulence model meets some extra difficulties, which will be discussed in Section 3.

2.2 A realization of a k-ε turbulence model

When dealing with three-dimensional flows at high Reynolds numbers, the numerical costs of DNS (Direct Numerical Simulation) are extremely high. To relax these costs, a k-ε turbulence model was recently added to FeatFlow, in order to allow the calculation of such flows on meshes of moderate size. The corresponding CFD code **Pp3d-Ke** was developed by D. Kuzmin building on the laminar FeatFlow version (http://www.featflow.de). The mathematical basis of this program can be described as follows.

We consider the following system of Navier-Stokes equations:

$$\begin{aligned} \frac{\partial \mathbf{u}}{\partial t} + \mathbf{u} \cdot \nabla \mathbf{u} &= -\nabla p + \nabla \cdot ((\nu_0 + \nu_{\mathrm{T}}) \mathcal{D}(\mathbf{u})) \,, \\ \nabla \cdot \mathbf{u} &= 0, \end{aligned} \tag{1}$$

where $\mathbf{u} = [u_1, u_2, u_3]^T$ is the averaged velocity, p is the averaged pressure, $\mathcal{D}(\mathbf{u}) = \frac{1}{2}\left(\nabla \mathbf{u} + (\nabla \mathbf{u})^T\right)$ is the strain tensor and $\nu_{\mathrm{T}} = C_\mu \frac{k^2}{\varepsilon}$ is the turbulent

viscosity. The turbulent kinetic energy k and its dissipation rate ε are modeled by two scalar transport equations:

$$\begin{aligned} \frac{\partial k}{\partial t} + \nabla \cdot \left(k\mathbf{u} - \frac{\nu_T}{\sigma_k}\nabla k \right) &= P_k - \varepsilon, \\ \frac{\partial \varepsilon}{\partial t} + \nabla \cdot \left(\varepsilon\mathbf{u} - \frac{\nu_T}{\sigma_\varepsilon}\nabla \varepsilon \right) &= \frac{\varepsilon}{k}(C_1 P_k - C_2 \varepsilon), \end{aligned} \tag{2}$$

where $P_k = \frac{\nu_T}{2}|\nabla \mathbf{u} + \nabla \mathbf{u}^T|^2$.

The equations contain some empirical constants for which the solver uses the default values $C_\mu = 0.09$, $C_1 = 1.44$, $C_2 = 1.92$, $\sigma_k = 1.0$, and $\sigma_\varepsilon = 1.3$.

Additionally, appropriate boundary conditions for $\mathbf{u}$, k and ε have to be prescribed on $\partial\Omega = \Gamma_{\text{in}} \cup \Gamma_{\text{out}} \cup \Gamma_{\text{wall}}$.

As usual, Dirichlet boundary conditions for $\mathbf{u}$, k and ε are prescribed on the inflow boundary Γ_{in}:

$$\mathbf{u} = \mathbf{g}, \quad k = c_{ab}|\mathbf{u}|^2, \quad \varepsilon = C_\mu \frac{k^{3/2}}{l_0}, \tag{3}$$

where c_{ab} is an empirical constant [KT04] and l_0 is a mixing length.

Let $(\mathbf{t}, \mathbf{n})$ be the local orthogonal basis for a wall node, where $\mathbf{t}$ and $\mathbf{n}$ are the tangential and normal directions, respectively. At the outlet Γ_{out} the following 'do-nothing' boundary conditions are prescribed:

$$\frac{\partial \mathbf{u}}{\partial \mathbf{n}} = 0, \quad \frac{\partial k}{\partial \mathbf{n}} = 0 \qquad \frac{\partial \varepsilon}{\partial \mathbf{n}} = 0, \quad \mathbf{n} \cdot [pI - \nu_T \mathcal{D}(\mathbf{u})] = 0. \tag{4}$$

In the k-ε model the behavior of a fluid near a solid wall is modeled by wall functions. The computational wall boundary Γ_{wall} is located at a distance δ from the real geometrical wall boundary. In our case we assume that the computational domain is already reduced by a layer of width δ, which is a user-defined parameter. Then we use the following boundary conditions on Γ_{wall}:

$$\mathbf{n} \cdot \mathbf{u} = 0, \quad \mathcal{D}(\mathbf{u}) \cdot \mathbf{n} = -\frac{u_\tau^2}{\nu_T}\frac{\mathbf{u}}{|\mathbf{u}|}, \quad k = \frac{u_\tau^2}{\sqrt{C_\mu}}, \quad \varepsilon = \frac{u_\tau^3}{\kappa\delta}, \tag{5}$$

where $\kappa = 0.41$ is the von Kármán constant and u_τ is the friction velocity, given here by the solution of the logarithmic wall law equation:

$$|\mathbf{u}| = u_\tau\left(\frac{1}{\kappa}\log y^+ + 5.5\right), \tag{6}$$

where $y^+ = \frac{u_\tau \delta}{\nu}$ is the local Reynolds number.

The discretization in space is performed by a finite element method using unstructured grids [Tur99]. A detailed description of the numerical algorithm for the k-ε model can be found in [KT04], [KLT05].

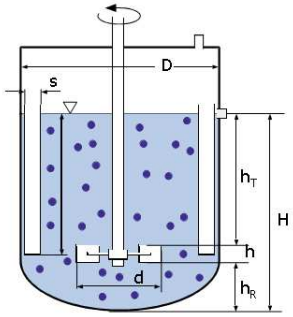

Figure 1: Stirred liquid-liquid system.

3 Simulation of stirred liquid-liquid systems

In this section, we consider a stirred liquid-liquid system, i. e. a stirred tank filled with two immiscible liquids that are stirred such that one liquid disperses into the other by building droplets, see Fig. 1. All droplets together are called the dispersed phase, whereas the other fluid is called the continuous phase.

3.1 Modeling

To model the relevant processes appearing in such a system, one has to account for the turbulent flow in the tank as well as for the population dynamical processes of the dispersed phase. In the discussed application, these latter processes are coalescence and breakage.

The flow field in the stirred tank is described by the Navier-Stokes equations for incompressible fluids, whereas the behavior of the drops is modeled by a population balance equation, where coalescence and breakage appear as source and sink terms on the right-hand side. Furthermore, turbulence is modeled by Reynolds-averaging and then solving the arising closure problem by using a k-ε turbulence model.

Remark 1 Let us discuss why it is useful to employ a k-ε turbulence model in this context. It is clear that some kind of turbulence modeling has to be used, since, otherwise the grid for the numerical calculation must be extremely fine to resolve the small eddies. For a 3D simulation of the stirred tank reactor with Reynolds number $\mathrm{Re} = 30,000$ this would require about $\mathrm{Re}^{\frac{9}{4}} \geq 10,000,000,000$ nodes (see e. g. [GDN98]), which is not feasible with today's computing power.

The k-ε turbulence model is natural in this context, since the quantity ε is needed anyway in the models for the coalescence and breakage processes.

If we assume that the drops do not have any influence on the flow field (they are just moving with the fluid with the same velocity), then the system of equations describing the processes in a stirred tank reactor is given by the Reynold-averaged Navier-Stokes equations (1) together with the transport equations for k and ε (2) from the k-ε turbulence model, and an averaged population balance equation, given by:

$$\begin{aligned}\frac{\partial f(\mathbf{x},V,t)}{\partial t} + \nabla\cdot(\mathbf{u}f(\mathbf{x},V,t)) - \nabla\cdot(c_t\nabla f(\mathbf{x},V,t)) \\ = s^+_{\text{coal}}(\mathbf{x},V,t) + s^-_{\text{coal}}(\mathbf{x},V,t) + s^+_{\text{break}}(\mathbf{x},V,t) + s^-_{\text{break}}(\mathbf{x},V,t), \quad (7)\end{aligned}$$

where $f(\mathbf{x},V,t)$ is the averaged number density function, which is not only dependent on the space coordinates $\mathbf{x}$ and the time t, but also on the drop volume V. The coaleascence and breakup phenomena are taken into account by means of the terms in the right-hand side of this integro-differential equation. The terms due to coalescence $s^{\pm}_{\text{coal}}(\mathbf{x},V,t)$ are modeled by

$$\begin{aligned} s^+_{\text{coal}}(\mathbf{x},V,t) &= \int_0^V R_{\text{coal}}(V',V'',\mathbf{y}(\mathbf{x},t))f(\mathbf{x},V',t)f(\mathbf{x},V'',t)dV', \\ s^-_{\text{coal}}(\mathbf{x},V,t) &= -f(\mathbf{x},V,t)\int_0^{V_{\max}-V} R_{\text{coal}}(V,V',\mathbf{y}(\mathbf{x},t))f(\mathbf{x},V',t)dV'. \end{aligned}$$

Here, $R_{\text{coal}}(V',V'',\mathbf{y}(\mathbf{x},t))$ denotes the coalescence rate, which describes the probability that two drops with volumes V' and V'' coalesce. The vector $\mathbf{y}$ is the so-called continuous phase vector (see e. g. [Ram00]), which is dependent on the properties of the continuous phase that influence the coalescence and breakage processes. Thus, the vector $\mathbf{y}$ may consist of pressure, temperature, or other values that we get from the calculation of the flow field.
On the other hand, the source and sink terms due to breakage $s^{\pm}_{\text{break}}(\mathbf{x},V,t)$ are modeled by:

$$\begin{aligned} s^+_{\text{break}}(\mathbf{x},V,t) &= \int_V^{V_{\max}} n(V',\mathbf{y}(\mathbf{x},t))\gamma(V,V',\mathbf{y}(\mathbf{x},t))R_{\text{break}}(V',\mathbf{y}(\mathbf{x},t)) \\ &\qquad f(\mathbf{x},V',t)dV', \\ s^-_{\text{break}}(\mathbf{x},V,t) &= -R_{\text{break}}(V,\mathbf{y}(\mathbf{x},t))\, f(\mathbf{x},V,t). \end{aligned}$$

Here, $R_{\text{break}}(V',\mathbf{y}(\mathbf{x},t))$ denotes the breakage rate, which accounts for the probability that a drop with volume V' breaks up. Furthermore, $\gamma(V,V',\mathbf{y}(\mathbf{x},t))$, the so-called distribution of daughter drops, describes the probability that the breakage of a drop with volume V' leads to at least one daughter drop with volume V. The quantity $n(V',\mathbf{y}(\mathbf{x},t))$ gives the number of daughter drops that are formed by the breakage of a drop with volume V'.

Physically, the following boundary conditions should be prescribed on $\Gamma_{\text{wall}} = \Gamma_{\text{stirrer}} \cup \Gamma_{\text{tank}}$:

$$\begin{aligned} \mathbf{u} &= \mathbf{u}_{\text{stirrer}} \text{ on } \Gamma_{\text{stirrer}}, \\ \mathbf{u} &= 0 \text{ on } \Gamma_{\text{tank}}, \\ f(\mathbf{x},V,t) &= 0 \text{ on } \Gamma, \end{aligned}$$

where Γ_{stirrer} describes the stirrer, and Γ_{tank} the boundary of the tank. Note that, for simplicity, the tank is modeled with a lid on top of it. Here, $\mathbf{n} = [\mathbf{n}_1, \mathbf{n}_2, \mathbf{n}_3]^T$ denotes the outer normal vector. The prescribed velocity on the stirrer $\mathbf{u}_{\text{stirrer}}$ is given by

$$\mathbf{u}_{\text{stirrer}} = [-r\sin(\varphi)\omega, r\cos(\varphi)\omega, 0]^T,$$

where $r = \sqrt{x_1^2 + x_2^2}$ is the radius, $\varphi = \arccos\left(\frac{x_1}{r}\right)$ is the angle, and ω is the constant angular velocity. This angular velocity is determined by the adjusted rotational speed N^* of the impeller. This parameter can be used as a control input in order to influence the drop size distribution. The initial conditions are chosen such that they are consistent with the boundary conditions. Further details about the modeling of stirred liquid-liquid systems can be found in [Sch04].

Setting of boundary conditions for the k-ε turbulence model with moving boundary parts has its own features, which we consider more precisely in 3.3.

3.2 Simulation approach

In this subsection, we will discuss how the system of equations (1-7) can be solved numerically. For the analysis, it is instructive to start with a brief analysis of the underlying differential-algebraic system, which we obtain after space-discretization, which describes the dynamics of the process. This analysis gives an indication of some of the numerical problems that may arise.

In [Sch04], it was shown that under the considered one-way coupling, the differentiation-index, see [CG95, KM06], of the differential-algebraic system that corresponds to the equations (1-7), which describe the processes in the stirred tank reactor, is two. This means that the index of the Navier-Stokes equations is not increased by the coupling with the population balance equation. Thus, all time integration schemes that are suitable for the solution of the semi-discretized Navier-Stokes equations can, in principle, also be used for solving the discussed coupled system.

Let us now discuss how the numerical simulation of the coupled system can be realized. In principle, the best way to treat the arising system of equations is to solve all the equations together as one coupled system (the so-called monolithic model). However, the effort to implement such a solver is immense, and thus this approach is currently not feasible in a short-term construction of a solver to be used in practical applications. For this reason we discuss the coupling of existing solvers, which is known as “co-simulation”. For this, already developed and implemented methods are combined via a relaxation method. This means that in each iteration step one method uses the results of a previous step of the other method and vice versa.
In this paper, we will apply this approach to solve the coupled system using the CFD code FeatFlow for the flow simulation and the solver Parsival [Wul] for the calculation of the drop size distribution.

As in the physical system, we consider a "one-way-coupling", i. e. we only consider the influence of the flow field on the drop size distribution and we only use the results of the CFD simulation for the calculation of the drop size distributions in each time step.

Using the recently implemented k-ε model also for the coupling between FeatFlow and Parsival, this coupling approach can be realized as follows. In a first step, the flow field as well as the turbulence parameters are calculated by FeatFlow using a very fine grid with several millions of cells. Since it is too costly to use just as many cells for the simulation of the drop size distributions, several cells are combined to one compartment so that for each compartment the drop size distribution can be calculated with Parsival. Within these compartments, the drop size distribution is assumed to be space-independent, and the compartments are chosen in such a way that this is approximately satisfied.

As next step, we implement a reactor consisting of l compartments in Parsival. In every time step, the mean energy dissipation rate $\bar{\varepsilon}_i$ for each compartment K_i is read from a file containing the CFD results such that the changes of the drop size distribution due to coalescence and breakage can be calculated. The mean energy dissipation rate $\bar{\varepsilon}_i(t)$ in compartment K_i is computed from the value $\varepsilon(x,t)$ that we get from the CFD calculation:

$$\bar{\varepsilon}_i(t) = \frac{1}{V_i} \int_{V_i} \varepsilon(\mathbf{x},t)\, d\mathbf{x}, \tag{8}$$

where V_i denotes the volume of compartment K_i. Furthermore, the average volume flow $\dot{V}_{ij}(t)$ between two neighboring compartments K_i and K_j is calculated via

$$\dot{V}_{ij}(t) = \max\big\{\, 0,\ \int_{A_{ij}} \mathbf{u}(\mathbf{x},t)\cdot\mathbf{n}_{ij}\, d\mathbf{x} \,\big\}, \tag{9}$$

where $\mathbf{u}(\mathbf{x},t)$ is the velocity calculated by FeatFlow, A_{ij} denotes the area of the face lying between the two compartments K_i and K_j, and $\mathbf{n}_{ij}$ denotes the unit normal vector on A_{ij} in direction from compartment K_i to compartment K_j. With these volume flows the convective flow of the drop size distributions is modeled. In time step $t = t_{k+1}$, we get the new distribution $f_i(t_{k+1})$ in compartment K_i from

$$f_i(t_{k+1}) = f_i(t_k) \ + \sum_{j \text{ neighbor of } i} \frac{\dot{V}_{ji}(t_k)}{V_i}\, f_j(t_k) \ - \sum_{j \text{ neighbor of } i} \frac{\dot{V}_{ij}(t_k)}{V_i}\, f_i(t_k).$$

3.3 Realization of the coupling

The coupling between the two simulators as described in the previous subsection is still not completely satisfactory. This is due to the fact that the implementation of the considered configuration in FeatFlow leads to some difficulties that have to be considered in more details. A first observation is that the fictitious

boundary method requires a very fine mesh in the area where the propeller its rotating. If this mesh is too coarse, then the very thin propeller blades are prescribed very inaccurately. This gives rise to large undesired errors in the calculation of the velocity field.

The second difficulty arises from the fact that the available time wall boundary laws for the k-ε turbulence model that were derived from physical experiments of channel flows require the boundary to be smooth and very plane.

Taking into the consideration these observations and assuming that major changes in the velocity vector field in the stirred tank reactor are due to the propeller, we come to the conclusion that it is preferable to perform a coordinate transformation using a fixed propeller around which the outside wall of the tank is rotating. Using this transformation, the system of Reynolds-averaged Navier-Stokes equations turns into

$$\begin{aligned} \frac{\partial \mathbf{u}}{\partial t} + \mathbf{u}\cdot\nabla\mathbf{u} &= -\nabla p + \nabla\cdot((\nu_0+\nu_\mathrm{T})\mathcal{D}(\mathbf{u})) - 2\boldsymbol{\omega}\times\mathbf{u} - \boldsymbol{\omega}\times(\boldsymbol{\omega}\times\boldsymbol{r}),\\ \nabla\cdot\mathbf{u} &= 0, \end{aligned}$$

where $\boldsymbol{\omega}$ is an angular velocity vector of the stirred tank reactor, $\boldsymbol{r}$ is a radius vector from the origin to the certain point, $2\boldsymbol{\omega}\times\mathbf{u}$ and $\boldsymbol{\omega}\times(\boldsymbol{\omega}\times\boldsymbol{r})$ are the Coriolis and centrifugal forces, respectively.

Using

$$\boldsymbol{\omega}\times\ (\boldsymbol{\omega}\times\mathbf{r}) = -\nabla\frac{(\boldsymbol{\omega}\times\mathbf{r})^2}{2}$$

and setting $P = p - \frac{1}{2}(\boldsymbol{\omega}\times\mathbf{r})^2$ yields the system

$$\begin{aligned} \frac{\partial \mathbf{u}}{\partial t} + \mathbf{u}\cdot\nabla\mathbf{u} &= -\nabla P + \nabla\cdot((\nu_0+\nu_\mathrm{T})\mathcal{D}(\mathbf{u})) - 2\boldsymbol{\omega}\times\mathbf{u},\\ \nabla\cdot\mathbf{u} &= 0. \end{aligned}$$

When solving this system, we have to be careful that the real pressure p has to be calculated from the transformed 'pressure' P. Furthermore, if the rotation is fast, i.e., the Eckmann number $Ek := \frac{\nu}{\omega L^2} \ll 1$, where L is a characteristic length, is large, then inertial forces dominate viscous forces and it may happen that the simulation diverges, see [Cod99], [Cod01].

Finally, we have to consider the boundary conditions in this setting. The given wall boundary conditions (5) in the k-ε turbulence model, which are prescribed everywhere on the solid wall are not sufficient, since we are not able to deal with $\mathbf{u} - \mathbf{u}\cdot\mathbf{n}$ (the tangential part of the velocity vector field) on the boundary. This problem can be overcome by realizing generalized boundary conditions according to [KFT00] and [JD92].

Due to the described difficulties that are currently being addressed, the coupling between FeatFlow and Parsival is currently still done without a turbulence

model. For the simulation of the drop size distributions with PARSIVAL, the results of the CFD simulation are used only for the volume flows between the compartments whereas for the mean energy dissipation rates $\bar{\varepsilon}_i$ values from the literature and experimental investigations are used.

Theoretically, if we were not face the difficulties discussed in Remark 1, the coupling between FEATFLOW and PARSIVAL could also be realized without turbulence model. In this case, the energy dissipation rate ε has to be calculated by its definition

$$\varepsilon := \frac{\nu}{2}\langle \|\nabla \mathbf{u}' + (\nabla \mathbf{u}')^T\|_F^2 \rangle,$$

where the values of the fluctuations

$$\mathbf{u}' = \mathbf{u} - \bar{\mathbf{u}} \quad \text{with} \quad \bar{\mathbf{u}} = \frac{1}{t_0}\int_{t-\frac{t_0}{2}}^{t+\frac{t_0}{2}} \mathbf{u}(\tau)d\tau$$

can be obtained by the results of the DNS.

However, in practice, this approach is usually very inaccurate, at least if post-processing is used for the calculation of ε from the simulated velocity field $\mathbf{u}$, which is then only given for a finite number of nodes. This typically leads to large approximation errors, in particular, in the calculation of the derivatives.

3.4 Simulation results

In the following, we will present the results of the simulation of the flow field with FEATFLOW as well as of the coupling with PARSIVAL.

3.4.1 Simulation of the flow field

The flow field in the stirred tank was simulated with FEATFLOW. The simulations were done for a stirred tank with torispherical head equipped with a six-bladed Rushton turbine and four baffles. Fig. 2 shows the grid consisting of about 2.8 million elements (hexahedrons) that was used for the simulation. The figure also shows the geometry of the tank and of the impeller. The tank has a height of $H_{\text{tank}} = 0.15\,m$ and the same diameter $D_{\text{tank}} = H_{\text{tank}}$. The impeller has a diameter of $D_{\text{imp}} = \frac{1}{3}D_{\text{tank}}$ and is located at height $H_{\text{imp}} = \frac{1}{3}H_{\text{tank}}$. The blades of the stirrer are $0.012\,m$ wide, $0.01\,m$ high, and $0.001\,m$ thick. The center disk has a diameter of $0.038\,m$ and a thickness of $0.001\,m$. The shaft is $0.009\,m$ in diameter, and the hub has a diameter of $0.013\,m$. The baffles are $0.013\,m$ wide, $0.1\,m$ high, and $0.001\,m$ thick and placed at a distance of $0.003\,m$ from the outer wall.

Fig. 3 shows the flow field in the stirred tank for Reynolds number $\text{Re} = 30,000$, which corresponds to a maximal prescribed velocity of $v_0 = 1.885\,{}^{m}/_{s}$ at the tip of the blades. Furthermore, Dirichlet-zero boundary conditions were prescribed on the whole boundary of the tank as well as on the four baffles.

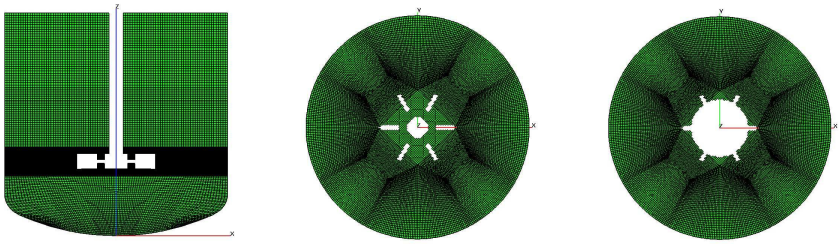

Figure 2: Grid used for the flow simulation with FeatFlow consisting of about 2.8 million elements. Left: longitudinal section, middle: cross section through the blades, above / below the disk, right: cross section through the disk.

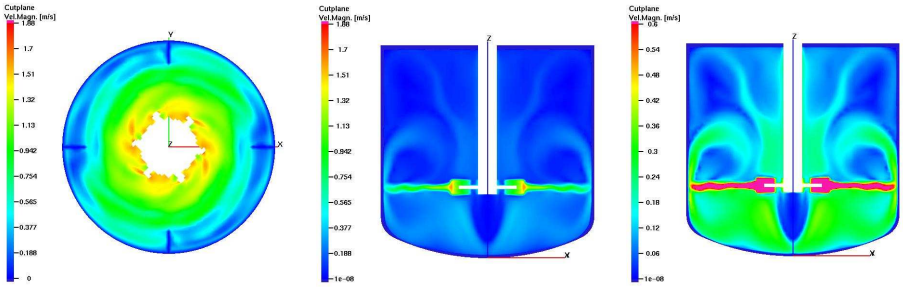

Figure 3: Flow field in the stirred tank for Re = 30,000. Left: cross section, middle: longitudinal section, right: longitudinal section, scaled plot.

In the left picture of Fig. 3, one sees a cross section of the velocity magnitude at height $H_{\text{tank}}/3$, i. e. directly through the blades and through the disk. This picture shows that the highest velocities occur, as expected, directly at the blades. Here, the fluid is moved with the stirrer, whereas near the wall or at the baffles the velocity of the fluid decreases down to zero.
In the middle picture, a longitudinal section of the velocity magnitude is shown. In this section, one observes the typical, so-called "drussy" shape of the flow field: The fluid is first moved outwards in radial direction, then splits up, when the boundary of the tank is reached, and flows back building two circles, one above and one below the impeller.
On the right-hand side in Fig. 3, a scaled plot of the velocity magnitude is depicted. By this scaling, the flow field in the regions more far away from the impeller can be seen better.
All three pictures show the flow field after about $t = 3.68\,s$, which corresponds to about 44 revolutions. After this time, the flow field is fully developed.

Altogether, one can say that, in the whole, the "mainstream" of the flow field is reproduced well by the simulation. However, if we have a more detailed look at the results, then we observe several regions, where the flow field is not calculated correctly. First, the width of the outwards flow in radial direction seems to be too small. In addition, it is not clear if the "wiggling" of this flow can be counted as turbulence or if it is an artifact caused by the numerics. Second, the velocity gradients are too high in the region below the stirrer, and also the amplitude of the velocity magnitude in this area seems to be to small.
Finally, also the gradients of the velocity at the boundary of the tank seem to be too high. A reason for this may be the fact that the grid is too coarse to resolve the boundary layer.

A detailed analysis of the results as well as a comparison with data from the literature is under investigation. However, by now, one can already say that either a finer grid or turbulence modeling is required in order to improve the results, see also Section 4.

3.4.2 Division of the tank into compartments

As already mentioned in Subsection 3.2, we cannot use the same fine grid for the calculation of the drop size distributions as for the flow simulation. The reason for this is that the population balance equation is not only dependent on space and time, but also on at least one internal coordinate that characterizes the elements of the dispersed phase (like the drop volume V in the considered application).

Since each additional coordinate increases the dimension of the problem, in many applications one uses the assumption of an ideally mixed tank. This means that the drop size distribution is assumed to be space-independent. However, due to the locally strong varying energy consumption throughout the tank, it is sensible to subdivide the domain at least into a few subdomains, the so-called

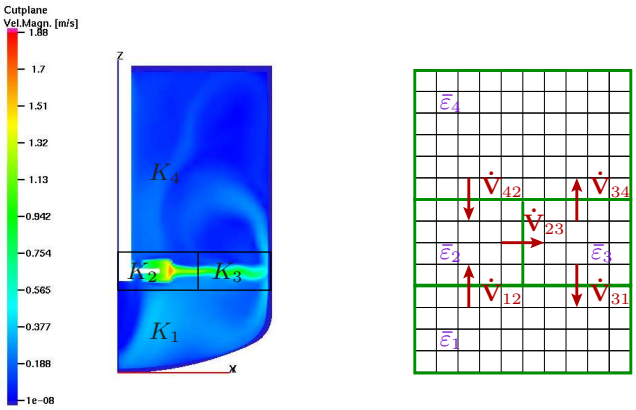

Figure 4: Left: division of the tank into four compartments $K_1, \ldots, K_4$ due to the velocity field. Right: Four-zone model with mean volume flows $\dot{V}_{ij}$ and mean energy dissipation rates $\bar{\varepsilon}_i$ drawn schematically.

compartments (which can be interpreted as a very coarse space discretization). This division is done according to the flow field that we get from the CFD simulation.

For the simulation with PARSIVAL, the tank is divided into four compartments as shown in Fig. 4, where only one half of the tank is shown. Compartment K_2, which lies directly around the stirrer, has the highest energy consumption, followed by compartment K_3, which is located in the same height, but in the outer part of the tank. Below and above these two compartments, respectively, there are the other two compartments K_1 and K_4, where the energy consumption is much smaller.

3.4.3 Calculation of the mean volume flows $\dot{V}_{ij}$

The next step is the calculation of the mean volume flows between neighboring compartments from the velocities derived by the flow simulation. Theoretically, these volume flows $\dot{V}_{ij}$ can be calculated by Eq. (9). However, in practice, we have to approximate the integral by a sum over given velocities:

$$\int_{A_{ij}} \mathbf{u}(\mathbf{x},t)\mathbf{n}_{ij}\, d\mathbf{x} \approx \sum_{\alpha=1}^{N} \mathbf{u}_\alpha(t)\mathbf{n}_{ij}\, A_\alpha,$$

where N is the total number of nodes on face A_{ij}. Here, $\mathbf{u}_\alpha$ denotes the velocity in node α and A_α denotes the area of the part of the face A_{ij} that belongs to node α. If we assume the grid to be equidistant, then we can use the approximation

$$\int_{A_{ij}} \mathbf{u}(\mathbf{x},t)\mathbf{n}_{ij}\, d\mathbf{x} \approx \sum_{\alpha=1}^{N} \mathbf{u}_\alpha(t)\mathbf{n}_{ij}\, A_\alpha = \frac{A_{ij}}{N} \sum_{\alpha=1}^{N} \mathbf{u}_\alpha(t)\mathbf{n}_{ij}. \tag{10}$$

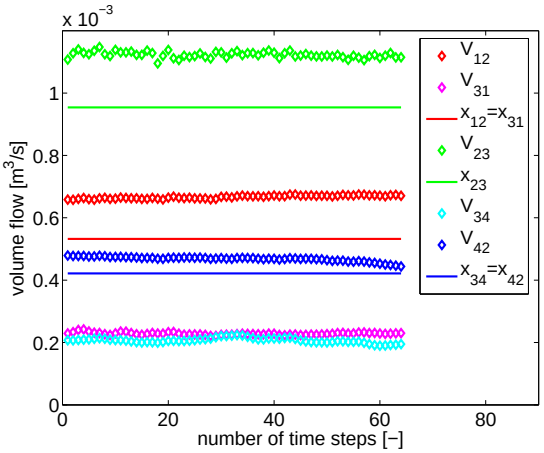

Figure 5: Volume flows between the four compartments. Values from CFD calculation (diamonds) and optimized values (solid lines).

The resulting volume flows calculated by Eq. (10) are shown in Fig. 5 (the diamonds). From Fig. 4 it can be seen that, due to the required mass conservation, the volume flows have to fulfill the conditions

$$\begin{aligned} \dot{V}_{31} - \dot{V}_{12} &= 0, \\ \dot{V}_{12} - \dot{V}_{23} + \dot{V}_{42} &= 0, \\ \dot{V}_{23} - \dot{V}_{31} - \dot{V}_{34} &= 0, \\ \dot{V}_{34} - \dot{V}_{42} &= 0. \end{aligned}$$

However, for the computed values in Fig. 5 these conditions are typically not satisfied.
There are several reasons for this. First of all, the grid used for the CFD simulation is not equidistant and, therefore, the assumption used in Eq. (10) is not fulfilled. However, this does not explain this significant deviation. Second, even if the grid was equidistant, the volume flows would not be calculated correctly, since FeatFlow does not control the conservation of mass for every cutplane, but only over the total domain.

To improve the calculation of these volumes one could use a more accurate interpolation formula, which takes the distance between two neighboring grid points into account so that the assumption of an equidistant grid could be avoided. However, the calculation of these distances is computationally too expensive for an unsorted list of about 2.8 million nodes. Another approach would be to choose the compartments for the calculation of the drop size distributions in such a way that they are composed of several cells of the coarse grid used for the CFD simulation. In this case, one would have the same number of nodes in each element of the coarse grid (due to the regular refinement of the grid). Thus, one could easily calculate the distance between two neighboring grid points (or at

least an average of it) within each element of the coarse grid. However, in the considered application, this approach cannot be used, since it is not possible to combine the elements of the coarse CFD grid in such a way that this leads to sensible compartments. An alternative would be to combine several cells of one of the finer grids used in the CFD simulation to obtain appropriate compartments. However, this would lead to very complicated boundaries between the different compartments, and, therefore, the calculations of the normal compounds of the velocities would be very complex.
This analysis shows that the best way would have been to create the coarse grid for the CFD simulation in such a way that an appropriate compartment model could be easily created by the combination of several coarse grid elements. However, the creation of such a "clever" grid consisting of quadrilateral elements is very sophisticated.

Since all the existent alternatives are either very complex and time-consuming or should have been applied in advance, it was decided to use the computed volume flows for the coupling and to fit them by applying the least-squares method. To do this, for the given volume flows $\dot{V}_{ij}^k$ between two compartments K_i and K_j at time t_k, we determine the optimal volume flows z_{ij}^k by solving the following minimization problem:

$$\|\mathbf{z}^k - \dot{\mathbf{V}}^k\|_2 = \text{min!} \quad \text{s.t.} \quad A\mathbf{z}^k = 0, \tag{11}$$

where $\mathbf{z}^k = [z_{12}^k, z_{23}^k, z_{31}^k, z_{34}^k, z_{42}^k]^T$, $\dot{\mathbf{V}}^k = [\dot{V}_{12}^k, \dot{V}_{23}^k, \dot{V}_{31}^k, \dot{V}_{34}^k, \dot{V}_{42}^k]^T$ for all time steps t_k, and A is given by

$$A = \begin{bmatrix} 1 & -1 & 0 & 0 & 1 \\ 0 & 1 & -1 & -1 & 0 \\ -1 & 0 & 1 & 0 & 0 \\ 0 & 0 & 0 & 1 & -1 \end{bmatrix}.$$

Since the volume flows $\dot{V}_{ij}^k$ do not change much in time (due to the constant stirrer speed), see also Fig. 5, it is more reasonable to solve the following minimization problem instead of (11),

$$\|\mathbf{z} - \dot{\mathbf{V}}^k\|_2 = \text{min!} \quad \text{for all time steps } t_k \quad \text{s.t.} \quad A\mathbf{z} = 0, \tag{12}$$

where $\mathbf{z} = [z_{12}, z_{23}, z_{31}, z_{34}, z_{42}]^T$. Here, $\mathbf{z}$ denotes the volume flows that are optimal with respect to the simulation results for all time points t_k. The latter formulation has the advantage that there are more data available for the calculation of the volume flows and as much information as possible is used for the calculation of the optimal values.

Fig. 5 shows the optimized volume flows (the solid lines) depending on the given volume flows $\dot{V}_{ij}^k$ (the diamonds), obtained by a FeatFlow simulation. Note that the axis of abscissae gives the number of time steps starting at some time point, when the flow field is already fully developed. The length of one time step is given by $\Delta t = 7.96 \cdot 10^{-3}\, s$.

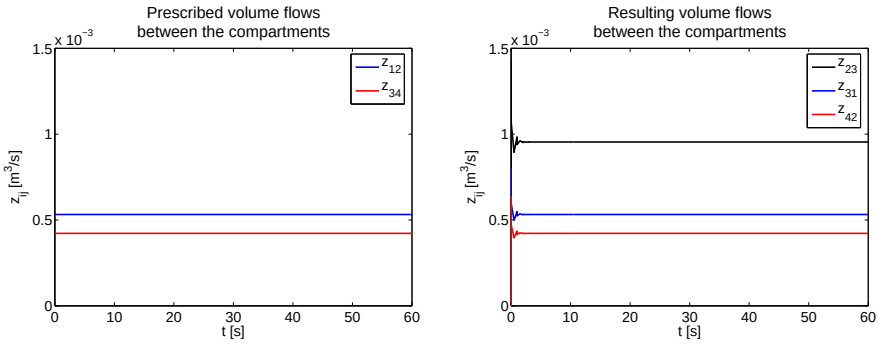

Figure 6: Volume flows between the different compartments. Left: prescribed volume flows z_{12} and z_{34}, right: resulting volume flows calculated by PARSIVAL.

3.4.4 Simulation of the drop size distributions

For the simulation of the drop size distributions with PARSIVAL, we have implemented a four-zone model, where the volume flows between the compartments are read from a file containing the calculated values z_{ij}, see Eq. (12). However, in PARSIVAL, only two of the five volume flows have to be prescribed, the other three are calculated by the program in such a way that mass is conserved, see Fig. 6.

For the description of the coalescence and breakage processes the model by Coulaloglou and Tavlarides [CT77] was used. The mean energy dissipation rates $\bar{\varepsilon}_i$ in the different compartments are chosen as follows:

$$\bar{\varepsilon}_1 = 0.329\,\bar{\varepsilon}, \quad \bar{\varepsilon}_2 = 12\,\bar{\varepsilon}, \quad \bar{\varepsilon}_3 = 2\,\bar{\varepsilon}, \quad \bar{\varepsilon}_4 = 0.3\,\bar{\varepsilon},$$

where $\bar{\varepsilon}$ denotes the overall mean value of the energy dissipation rate ε throughout the tank. By this choice, the turbulence distribution is as expected (and, at least roughly, as in the literature, see [AKK99]). Furthermore, the condition

$$\sum_{i=1}^{4} \bar{\varepsilon}_i V_i = \bar{\varepsilon}\, V_{\text{tank}}$$

is fulfilled. To determine $\bar{\varepsilon}$ we use

$$\bar{\varepsilon} = \frac{\text{Ne}\,(N^*)^3 (D_{\text{stirrer}})^5}{V_{\text{tank}}},$$

where Ne denotes the power number, D_{stirrer} is the diameter of the stirrer, and V_{tank} is the volume of the tank, see [Kra03]. For the considered application this formula gives $\bar{\varepsilon} = 1.18$, where we have used the value $\text{Ne} = 5.5$ for the power number.

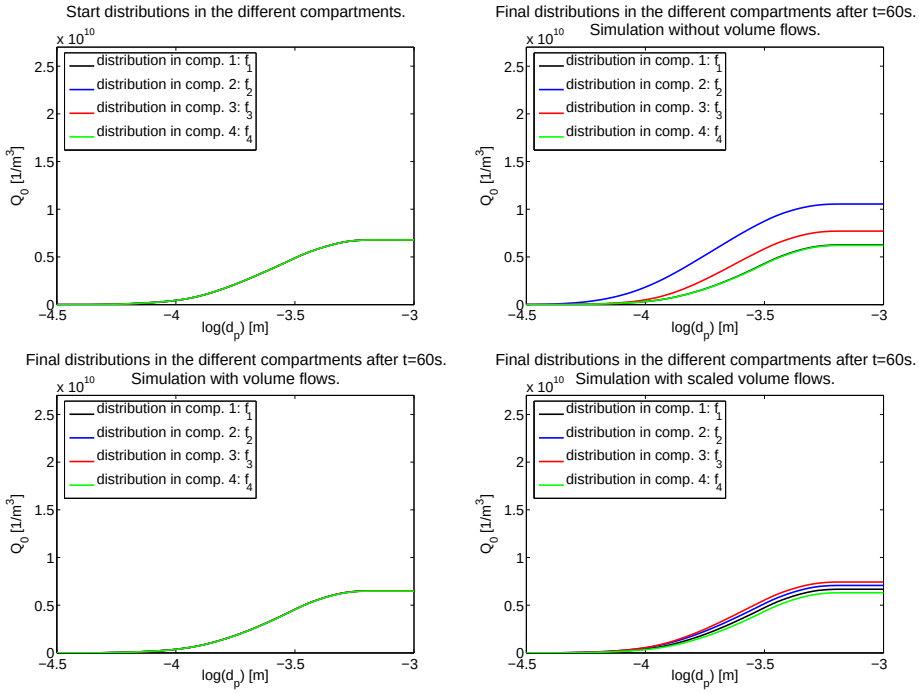

Figure 7: Drop size distributions in the different compartments. Top left: start distributions, top right: final distributions after $t = 60\,s$ for a simulation without volume flows between the compartments, bottom left: final distributions after $t = 60\,s$ for a simulation with volume flows, bottom right: final distributions after $t = 60\,s$ for a simulation with scaled volume flows.

Fig. 7 shows the resulting drop size distributions for the case that the same Gaussian normal distribution is used as initial condition in all four compartments. In the left top picture of Fig. 7, this arbitrarily chosen start distribution is depicted.
In the top right picture, one can see the final distributions after $t = 60\,s$ within the different compartments for the case that the simulation is done without volume flows between the compartments. Here one observes that the distributions in the first and in the fourth compartment are moved towards larger drop sizes. Thus, there are less, but larger drops after the simulation. The reason for this is that we have chosen relatively small values for the mean energy dissipation rates in these compartments. Thus, coalescence and breakage take place simultaneously, but coalescence dominates, which means that the number of coalescing drops is higher than the number of breaking drops. On the other hand, in the second compartment, where the mean energy dissipation rate has been chosen much higher than the average value, only breakage occurs. (The reason for this is that the drops are not able to stay in contact as long as coalescence needs to take place.) This effect results in a significant change of the distribution to smaller drop sizes. Therefore, in the second compartment, there are more and hence smaller drops. Also in compartment K_3, there are more and smaller drops after the simulation than before. Here, breakage dominates, since the mean energy dissipation rate in this compartment is twice as high as the overall mean value $\bar{\varepsilon}$.
In the bottom left picture, the final distributions in the different compartments after a simulation with volume flows are shown. Here, we have prescribed the optimized volume flows that we get from Eq. (12). One oberserves that in all compartments, the distributions are almost the same. The reason for this is that the volume flows are so high that they lead to a total exchange of the drop size distributions in the compartments. However, if we compare these drop size distributions with the prescribed start distribution, we see that there are fewer but bigger drops after $t = 60s$. An explanation for this is that the compartments K_1 and K_4, where we have prescribed relatively low values for the mean energy dissipation rates, are much bigger than the other two compartments.
In the bottom right picture the resulting drop size distributions for a simulation with smaller volume flows are depicted. Here, we have used volume flows that have been scaled by a factor of 0.01. In this case, the exchange between the compartments is not as high as before, and, thus, the influence of the volume flows on the drop size distributions in the different compartments can be seen better. The first thing that should be noted is that this time we find the most and smallest drops in compartment K_3 and not in compartment K_2, where we have prescribed the highest value for $\bar{\varepsilon}_i$. The reason for this is that the drops in compartment K_2 are directly transported to compartment K_3. Thus, the input into compartment K_3 consists only of "small" drops, whereas only larger drops are transported into compartment K_2. Another, at first sight surprising observation is that there are more and smaller drops in compartment K_1 than in compartment K_4, although we have prescribed almost the same values for $\bar{\varepsilon}_1$ and $\bar{\varepsilon}_4$. The reason for this is that compartment K_4 is much bigger than com-

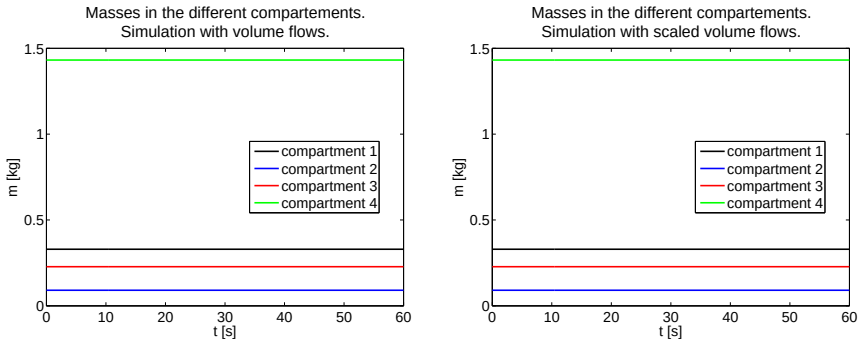

Figure 8: Conservation of mass during the simulation with PARSIVAL. Left: simulation with volume flows (corresponding to the left bottom picture in Fig. 7), right: simulation with scaled volume flows (corresponding to the right bottom picture in Fig. 7).

partment K_1 and, thus, the transported smaller drops from the compartments K_2 and K_3 do not carry so much weight there.

Fig. 8 shows that mass is conserved during the simulation with PARSIVAL. In the left picture, the masses in the different compartments are depicted for a simulation with volume flows in order of magnitude corresponding to the results of the CFD simulation, whereas in the right picture the masses for the scaled simulation are shown.

4 Discussion

The current simulation results show many challenges.
Obviously, the results of the flow simulation still need to be improved. However, if DNS is used, a much finer grid is required, which can clearly not be handled due to the high time and memory requirements for the simulation, even if a parallel CFD solver is used. So, at the moment, it is sensible to use some kind of turbulence modeling, which is currently being completed, see Section 2.
Further difficulties arise when the coupling with PARSIVAL is considered. It is quite complicated to find a sensible "connection" between the solvers as FEATFLOW is an open-source FORTRAN code whereas PARSIVAL is a commercial Windows program controlled by a graphical user interface.

At the moment a sensible adaption of the k-ε turbulence model solver **Pp3d-Ke** to the application of stirred liquid-liquid systems described in Section 3 is investigated, including the coordinate transformation described in the beginning of Subsection 3.3.
Despite all the difficulties in the implementation of the k-ε turbulence model in FEATFLOW, which arise in particular in the moving boundary parts, neverthe-

less the k-ε model seems to be particularly suitable for the presented coupling approach, since the energy dissipation rate ε, which is needed for the calculation of the coalescence and breakage rates, is directly provided by the CFD code.

References

[AKK99] V. Alopaeus, J. Koskinen, and K. I. Keskinen. Simulation of the population balances for liquid-liquid systems in a nonideal stirred tank. Part 1: Description and qualitative validation of the model. *Chemical Engineering Science*, 54:5887–5899, 1999.

[CG95] S. L. Campbell and C. W. Gear. The index of general nonlinear DAEs. *Numerische Mathematik*, 72:173–196, 1995.

[Cod99] R. Codina. Numerical solution of the incompressible Navier-Stokes equations with Coriolis forces based on the discretization of the total time derivative. *Journal of Computational Physics*, 148:467–496, 1999.

[Cod01] R. Codina. A stabilized finite element method for generalized stationary incompressible flows. *Comput. Methods Appl. Mech. Engrg.*, 190:2681–2706, 2001.

[CT77] C. A. Coulaloglou and L. L. Tavlarides. Description of interaction processes in agitated liquid-liquid dispersions. *Chemical Engineering Science*, 32:1298–1297, 1977.

[GDN98] M. Griebel, T. Dornseifer, and T. Neunhoeffer. *Numerical Simulation in Fluid Dynamics: A Practical Introduction*. SIAM Monographs on Mathematical Modeling and Computation. SIAM, Philadelphia, 1998.

[JD92] M. Jaeger and G. Dhatt. An extended $k - \varepsilon$ finite element model. *International Journal for Numerical methods in Fluids*, 14:1325–1345, 1992.

[KFT00] B. Koobus, C. Farhat, and H. Tran. Computation of unsteady viscous flows around moving bodies using the $k - \varepsilon$ turbulence model on unstructured dynamic grids. *Comput. Methods Appl. Mech. Engrg.*, 190:1441–1466, 2000.

[KLT05] D. Kuzmin, R. Löhner, and S. Turek. *Flux-Corrected Transport*. Springer, 2005.

[KM06] P. Kunkel and V. Mehrmann. *Differential-Algebraic Equations. Analysis and Numerical Solution*. EMS Publishing House, Zürich, Switzerland, 2006.

[Kra03] M. Kraume, editor. *Mischen und Rühren. Grundlagen und moderne Verfahren*. Wiley-VCH, Weinheim, 2003.

[KT04] D. Kuzmin and S. Turek. Numerical simulation of turbulent bubbly flows. *3rd International Symposium on Two-Phase Flow Modelling and Experimentation 2004*, Pisa, 2004.

[Ram00] D. Ramkrishna. *Population Balances. Theory and Applications to Particulate Systems in Engineering*. Academic Press, San Diego, 2000.

[Sch04] S. Schlauch. Modeling of stirred liquid-liquid dispersions. Preprint 41-2004, Institut für Mathematik, Technische Universität Berlin, 2004.

[TDR02] S. Turek, W. Decheng, and L. Rivkind. The fictitious boundary method for the implicit treatment of Dirichlet boundary conditions with applications to incompressible flow simulation. In E. Bänsch, editor, *Challenges in Scientific Computing CISC 2002*, LNCSE, pages 37–68, Berlin, 2002. Springer.

[Tur99] S. Turek. *Efficient Solvers for Incompressible Flow Problems: An Algorithmic and Computational Approach*. Lecture Notes in Computational Science and Engineering. Springer, Berlin, Heidelberg, New York, 1999.

[Wul] M. Wulkow. *PARSIVAL. Simulation Package for Particle Balances*. CiT GmbH.